Tri-band transparent cross-polarization converters using a chiral metasurface*

Shi Hong-Yu(施宏宇)[a], Li Jian-Xing(李建星)[a], Zhang An-Xue(张安学)[a]†,
Wang Jia-Fu(王甲富)[b], and Xu Zhuo(徐 卓)[c]

[a] School of Electronic and Information Engineering, Xi'an Jiaotong University, Xi'an 710049, China
[b] College of Science, Air Force Engineering University, Xi'an 710051, China
[c] Electronic Materials Research Laboratory, Xi'an Jiaotong University, Xi'an 710049, China

(Received 22 April 2014; revised manuscript received 14 May 2014; published online 24 September 2014)

A chiral metasurface is proposed to realize a tri-band polarization angle insensitive cross-polarization converter. The unit cell of the chiral metamaterial is composed by four twisted anisotropic structure pairs in four-fold rotation symmetry. The simulation results show that this device can work at 9.824 GHz, 11.39 GHz, and 13.37 GHz with low loss and a high polarization conversion ratio (PCR) of more than 99%. The proposed design can transmit the co-polarization wave at 14.215 GHz, like a frequency selective surface. The study of the current and electric fields distributions indicates that the cross-polarization transmission is due to electric dipole coupling.

Keywords: multi-band, polarization angle independent, optical activity, chiral metamaterials

PACS: 81.05.Xj, 41.20.Jb **DOI:** 10.1088/1674-1056/23/11/118101

1. Introduction

Controlling the propagation characteristics, including the polarization states, of electromagnetic waves has long been of concern.[1–3] Metamaterials can be used to realize cloaks,[4] lens,[5] absorbers,[6–9] polarizers,[10,11] and surface plasmon polariton couplers[12–14] to effectively manipulate the propagation of microwaves. Polarization is one of the most important properties of microwaves, which has aroused the interest of researchers.[15–17] Nowadays, much attention has been paid to the polarization rotation or optical activity,[18–21] and different types of cross-polarization converters have been designed.[22–25] To avoid interference effects between the incident and reflected waves, great efforts have been made to design transparent cross-polarization converters. Anisotropic and chiral metamaterials have been used to manipulate the propagation of the microwaves in different ways. Anisotropic metamaterials can cause a phase or amplitude difference between two crossed polarization waves, which can be used to manipulate the polarization of the incident waves. Pfeiffer *et al*. reported a 4-layered anisotropic structure to convert the polarization.[26] However, most transparent low-loss polarizers or cross-polarization converters that are based on anisotropic metamaterials are multi-layered structures, which cause a large thickness. Metasurfaces are single-layer metamaterials with scatters judiciously placed in a two-dimensional (2D) pattern at the surface or the interface. Chiral metasurfaces are also used to rotate the polarization angle of the microwaves by transverse magnetic dipole coupling. Liu *et al.* presented a chiral nanostructure to obtain huge optical activity.[18] Types of chiral metamaterials in microwave band have also been reported to convert polarization.[27–29] Although these chiral metasurfaces are thin, they usually work in single frequency or have a polarization sensitive response. Thus, it is desirable to research multi-band polarization angle-independent cross-polarization converters with high performance.

In this paper, we propose a tri-band cross-polarization converter using a chiral metasurface. The proposed cross-polarization converter has a polarization angle-independent response with a high polarization conversion ratio of more than 99%. The cross-polarization transmissions are caused by electric dipole coupling. The unit cell of the chiral metasurface is composed by four twisted anisotropic structure pairs, which is chiral, as shown in Fig. 1. The four anisotropic structure pairs are arranged in $C4$ rotation symmetry to obtain a polarization-independent response.[24] The measured results coincide with the simulation results and demonstrate that the proposed cross-polarization converter can work at 9.82 GHz, 11.39 GHz, and 13.37 GHz. Furthermore, the proposed chiral metasurface has a co-polarization transmission at 14.215 GHz, like a frequency selective surface.

2. Design of the cross-polarization converter

2.1. Structure of the chiral metasurface

Chiral structures have the potential to realize a cross-polarization converter.[30] It is assumed that the chiral metasurface is illuminated by a plane wave propagating along z direction

$$\boldsymbol{E}_i(\boldsymbol{r},t) = \begin{pmatrix} i_x \\ i_y \end{pmatrix} \mathrm{e}^{\mathrm{i}(kz-\omega t)}, \tag{1}$$

*Project supported by the National Natural Science Foundation of China (Grant Nos. 61331005, 61001039, and 41390454).
†Corresponding author. E-mail: anxuezhang@mail.xjtu.edu.cn
© 2014 Chinese Physical Society and IOP Publishing Ltd

with ω being its frequency, k being its wave number, and the complex amplitudes i_x and i_y describing the state of linear polarization. Thus, the transmitted fields is

$$\boldsymbol{E}_t(\boldsymbol{r},t) = \begin{pmatrix} t_x \\ t_y \end{pmatrix} \mathrm{e}^{\mathrm{i}(kz-\omega t)}. \tag{2}$$

After that, the transmission matrix (T matrix), which connects the incident fields and transmitted fields, is given by

$$\begin{pmatrix} t_x \\ t_y \end{pmatrix} = \begin{pmatrix} T_{xx} & T_{xy} \\ T_{yx} & T_{yy} \end{pmatrix} \begin{pmatrix} i_x \\ i_y \end{pmatrix}. \tag{3}$$

For those chiral structures exhibiting $C4$ symmetry but without any additional reflection symmetry, their T matrix in the linear base is

$$\boldsymbol{T}_{\mathrm{line}} = \begin{pmatrix} T_{xx} & T_{xy} \\ T_{yx} & T_{yy} \end{pmatrix}, \tag{4}$$

where the entries T_{ij} are complex amplitudes, and $T_{xx} = T_{yy}$ and $T_{xy} = -T_{yx}$.[31] Thus, the structure in $C4$ symmetry is insensitive to the polarization state of the linear wave. Then, the eigenbasis in matrix form is

$$\hat{\Lambda} = \begin{pmatrix} 1 & 1 \\ \dfrac{\kappa_1 - T_{xx}}{T_{xy}} & \dfrac{\kappa_2 - T_{xx}}{T_{xy}} \end{pmatrix} = \begin{pmatrix} 1 & 1 \\ j & -j \end{pmatrix},$$
$$\kappa_{1,2} = \frac{1}{2}\left[(T_{xx}+T_{yy}) \pm \sqrt{(T_{xx}-T_{yy})^2 + 4T_{xy}T_{yx}}\right]. \tag{5}$$

Thus, the eigenpolarizations of the chiral structures in $C4$ symmetry are a left- and right-handed circular polarization. In the circular base, the T matrix is

$$\boldsymbol{T}_{\mathrm{circ}} = \begin{pmatrix} T_{++} & 0 \\ 0 & T_{--} \end{pmatrix}, \tag{6}$$

where the entries T_{++} and T_{--} are complex amplitudes of the co-polarization transmission. Assuming that the incident wave is linearly polarized in any states, in order to realize a cross-polarization converter, the T_{++} and T_{--} should satisfy the condition of $T_{++} = -T_{--}$, and if $T_{++} = T_{--}$ then the chiral metasurface responses without any polarization transformation.

Considering the above analysis, in this paper we propose a chiral metasurface in $C4$ symmetry to realize a triband cross-polarization converter. The structure of the proposed chiral metasurface is shown in Fig. 1(a). The unit cell of the chiral metasurface is composed of four twisted anisotropic structure pairs which are arranged in $C4$ symmetry. The top layer and bottom layer structures in each anisotropic structure pair are mutually twisted by an angle of 45°, as shown in Figs. 1(b) and 1(c). The geometrical parameters of the structure are given by $l = 3.5$ mm, $s = 0.9$ mm, $g = 0.1$ mm, $w = 0.5$ mm, $w1 = 0.1$ mm, $r = 3.1$ mm, $h = 3.18$ mm, and $\Phi = 45°$. The periodic of the chiral metasurface unit cell structure is $p = 14$ mm, which avoids diffraction at the normal incidence for frequencies below 21 GHz. The dielectric constant and loss tangent of the substrate are 6.18 and 0.002, respectively.

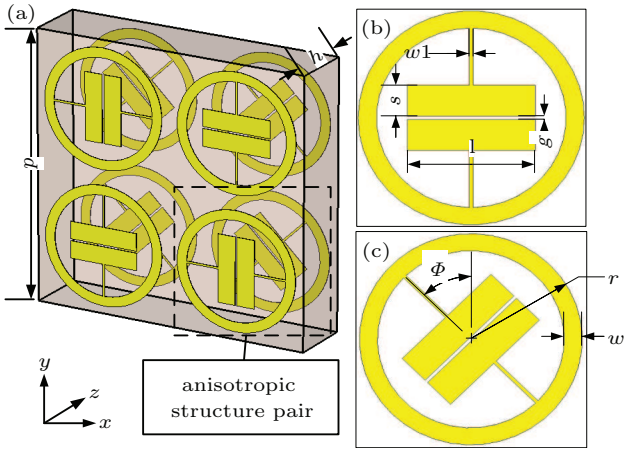


Fig. 1. (color online) (a) Geometry of the chiral metasurface unit cell; (b) the top layer of the structure; (c) the bottom layer of the structure.

2.2. Simulation results

In our simulations, we used the commercial software CST MICROWAVE STUDIO. The unit cell boundary condition is used along x and y directions, and the absorbing boundary condition is applied for the z direction. The model is excited by Folquet port with the normal incidence of circularly polarized and linearly polarized waves in a frequency range of 9 GHz–15 GHz.

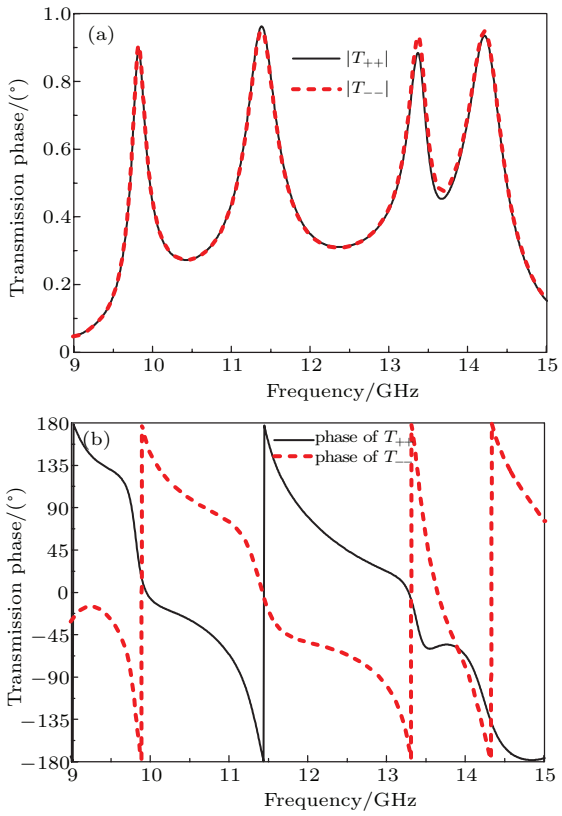


Fig. 2. (color online) (a) The transmission of the waves in the eigenpolarizations; (b) the phase difference of the transmitted waves in eigenpolarizations.

When illuminated by the waves of the eigenpolarizations (circular polarization), the designed chiral metasurface exhibits four transmission bands at 9.824 GHz, 11.39 GHz, 13.37 GHz, and 14.215 GHz, as shown in Fig. 2(a). Furthermore, the phase differences of the waves of the two cross eigenpolarizations at these four frequencies are 172.2°, 171°, 171.7° and 31.8°, as shown in Fig. 2(b). Thus, according to the theory in Section 2.1, the designed chiral metasurface will act as a cross-polarization converter at frequencies near 9.82 GHz, 11.39 GHz, and 13.37 GHz. Near 14.215 GHz, the proposed chiral metasurface will respond like a frequency selective surface.

To evaluate the characteristics of the designed cross-polarization converter, the situation at the illumination of linearly polarized waves is also simulated. Because the chiral metasurface is insensitive to the polarization state of the linear wave, only results at y-polarized wave illumination are plotted for simplicity. The simulated co-polarization transmission $|T_{yy}|$ and cross-polarization transmission $|T_{xy}|$ are plotted in Fig. 3(a). At 9.82 GHz, 11.39 GHz, and 13.37 GHz, the values of $|T_{xy}|$ are all larger than 0.9, and the values of $|T_{yy}|$ are all lower than 0.06.

The polarization conversion ratio (PCR), the polarization rotation azimuth angle ψ, and the ellipticity η are used to evaluate the performances of the proposed cross-polarization converter. The PCR is defined as

$$\mathrm{PCR} = |T_{xy}|^2 \Big/ \left(|T_{yy}|^2 + |T_{xy}|^2\right), \tag{7}$$

and the ψ and the η are

$$\psi = \frac{1}{2}\tan^{-1}\left\{\frac{2R\cos(\varphi)}{1-R^2}\right\}, \tag{8}$$

$$\eta = \frac{1}{2}\sin^{-1}\left\{\frac{2R\sin(\varphi)}{1+R^2}\right\}, \tag{9}$$

where $R = |T_{xy}|/|T_{yy}|$ and $\varphi = \arg(T_{xy}) - \arg(T_{yy})$. The PCR is plotted in Fig. 3(b), which shows that at 9.82 GHz, 11.39 GHz, and 13.37 GHz the PCRs are higher than 0.99, at 14.215 GHz, the PCR is 0.076. The polarization rotation azimuth angle ψ and the ellipticity η are shown in Figs. 4(a) and 4(b). At 9.82 GHz, 11.39 GHz, and 13.37 GHz, the simulated ψ are −86.95°, −86.62° and −89.56° and the simulated η are 0.265°, −0.063°, and −1.728°, respectively. The transmission, PCR, ψ and η are summarized in Table 1.

From the above results it can be seen that the transmitted wave is almost pure linearly polarized at the four transmission peaks, the polarization angles are rotated by nearly 90° at 9.82 GHz, 11.39 GHz, and 13.37 GHz. At 14.215 GHz, the polarization angle is rotated by only 16°.

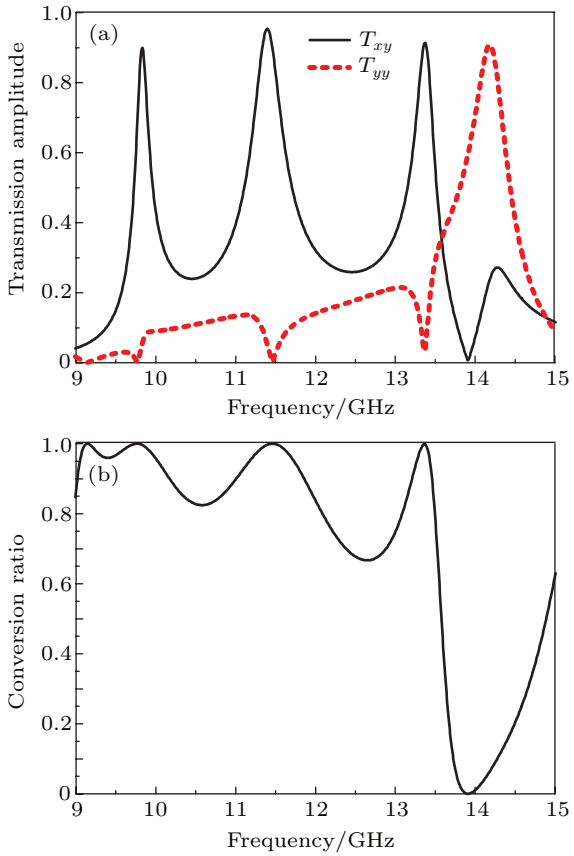


Fig. 3. (color online) (a) The simulated transmission power of co-polarization ($|T_{yy}|$) and cross-polarization ($|T_{xy}|$); (b) the polarization conversion ratio.

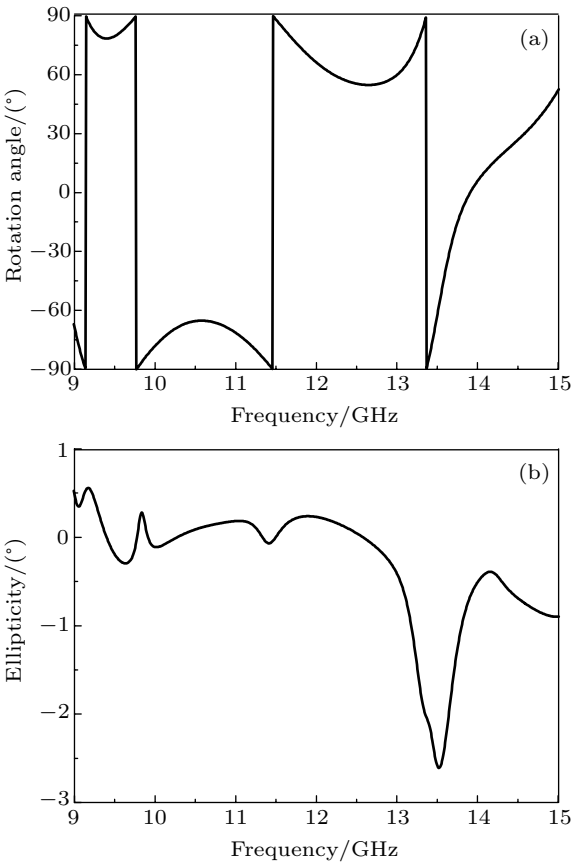


Fig. 4. (a) The polarization rotation angle; (b) the ellipticity.

Table 1. Summary of the properties of the chiral metasurface.

Frequency/GHz	9.824	11.39	13.37	14.215
$\|T_{xy}\|$	0.9	0.95	0.92	0.23
$\|T_{yy}\|$	0.052	0.052	0.037	0.91
PCR	0.997	0.996	0.998	0.076
$\psi/(^\circ)$	−86.95	−86.62	−89.56	16
$\eta/(^\circ)$	0.265	−0.063	−1.728	−0.412

2.3. Discussion of the cross-polarization converter

In order to obtain a physical insight into the behavior of the proposed design, we have observed the surface current distributions on both the top layer and the bottom layer of the chiral metasurface, as well as the electric field in the substrate. Because the unit cell of the chiral metasurface is $C4$ symmetric, the current distributions and fields on the diagonal structures are the same. Therefore, only the currents on the two anisotropic pairs in the first row of the unit cell are shown for simplicity.

At 9.824 GHz, the cross-polarization transmission is due to the electrical dipole coupling. Figures 5(a) and 5(b) show the current distributions on the top layer and bottom layer of the chiral metasurface, respectively. On the left or right side of each anisotropic structure, the currents on the top layer (in Fig. 5(a)) and bottom layer (in Fig. 5(b)) are antiparallel, which are induced by the incident magnetic fields along x direction. However, these currents induce additional currents inside the metal loop, which cause the parallel electrical dipoles along x direction, and then generate the cross polarization fields, as shown in Fig. 5(c).

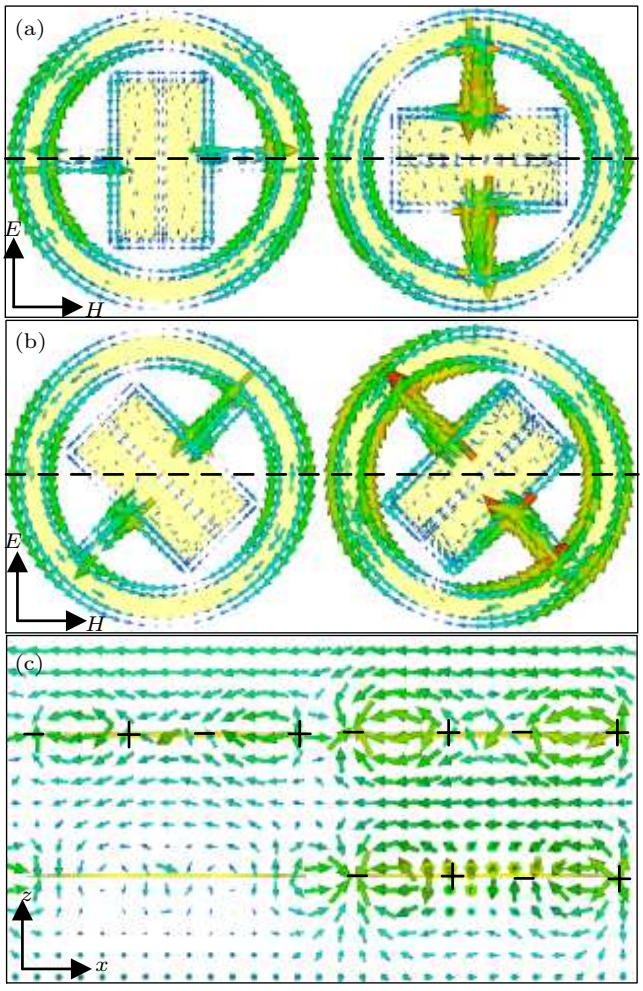


Fig. 5. (color online) (a) and (b) The current distributions on the top layer and the bottom layer of the chiral metasurface at 9.824 GHz. (c) The electric field on the cut plane indicated by the dashed lines in panels (a) and (b).

The cross-polarization transmission at 11.39 GHz is also due to the electrical dipole coupling, but in a different mode. The current distributions on the top layer and bottom layer of the chiral metasurface are plotted in Figs. 6(a) and 6(b), respectively. On left or right side of each anisotropic structure, the currents on the top layer (Fig. 6(a)) and bottom layer (Fig. 6(b)) are parallel, which are induced by the incident electric fields along y direction. By electromagnetic coupling, parallel electrical dipoles along x direction are induced, and these electrical dipoles contribute to the cross-polarization transmission, as shown in Fig. 6(c).

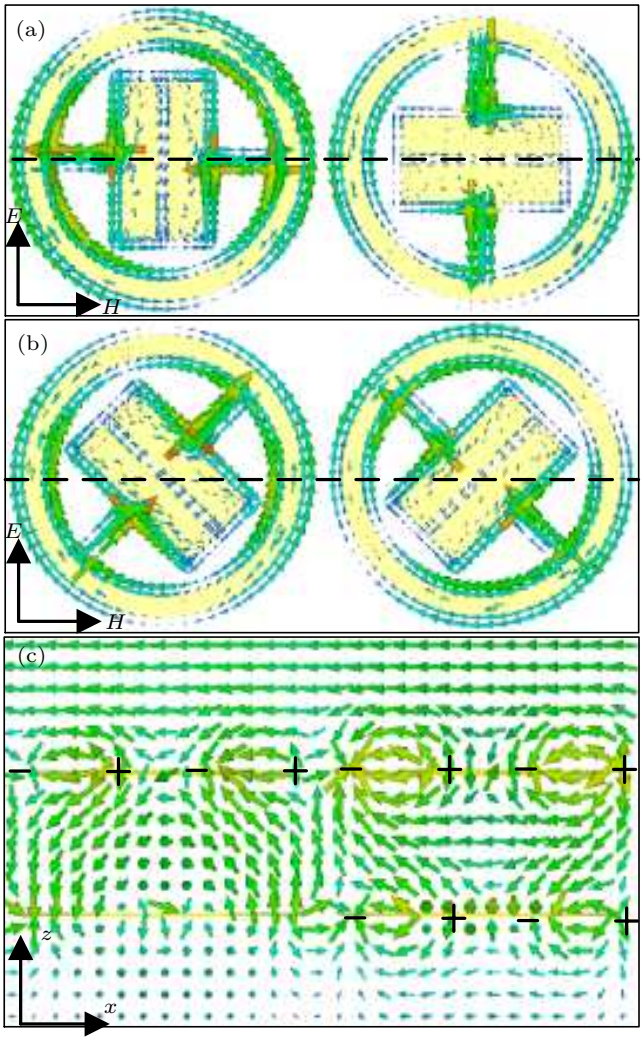


Fig. 6. (color online) (a) and (b) The current distributions on the top layer and the bottom layer of the chiral metasurface at 11.39 GHz. (c) The electric field on the cut plane indicated by the dashed lines in panels (a) and (b).

At 13.37 GHz, the cut wires inside the metal loop are strongly excited by the incident wave, as shown in Figs. 7(a)

and 7(b). However, transverse electrical dipoles along x direction are induced by these strong currents, and these electrical dipoles strongly contribute to the cross-polarization transmission, as shown in Fig. 7(c). Notably, on the up or down side of each anisotropic structure, parallel currents in x direction are induced on the top layer (in Fig. 7(a)) and bottom layer (in Fig. 7(b)). Although the currents on the up or down side of the left structure and right structure are antiparallel, the currents on the left structure are much stronger than those on the right structure. Thus, there are net currents along x direction, which also contribute to the cross-polarization transmission.

The current distribution and electrical field at 14.215 GHz are plotted in Fig. 8. Antiparallel currents are induced on the metal loop, so their effects are canceled. The currents inside the metal loop create electrical dipoles along x direction; however, the electrical dipoles on left and right structures are antiparallel. Thus, these electrical dipoles generate negligible electric fields along x direction, and the transmission at 14.215 GHz is co-polarized.

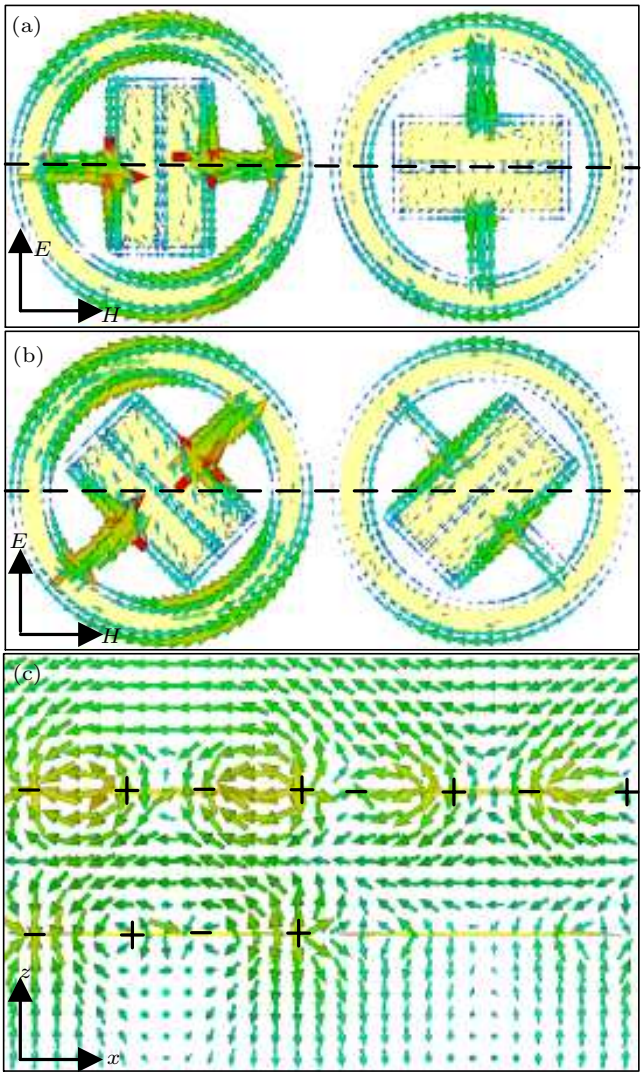


Fig. 7. (color online) (a) and (b) The current distributions on the top layer and the bottom layer of the chiral metasurface at 13.37 GHz. (c) The electric field on the cut plane indicated by the dashed lines in panels (a) and (b).

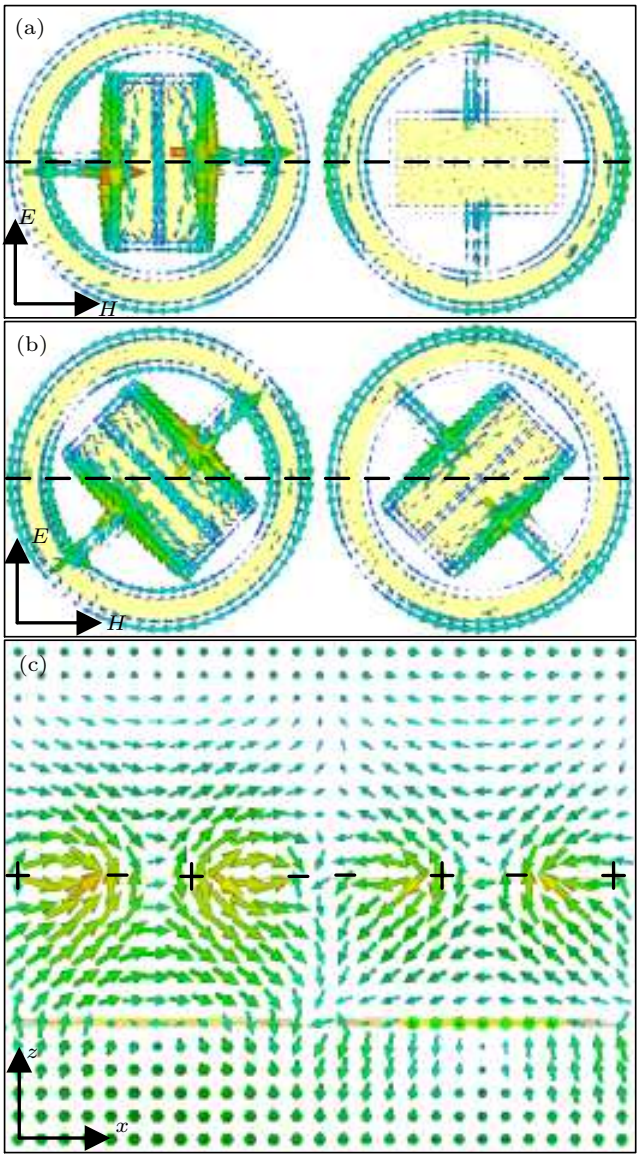


Fig. 8. (color online) (a) and (b) The current distributions on the top layer and the bottom layer of the chiral metasurface at 14.215 GHz. (c) The electric field on the cut plane indicated by the dashed lines in panels (a) and (b).

3. Experimental results

To further verify the designed chiral metasurface, a sample with outer dimensions of 280 mm × 280 mm is fabricated, as shown in Fig. 9. The thickness h of the substrate is 3.18 mm and the dielectric constant and loss tangent are 6.15 and 0.002, respectively. The measurement results are shown in Figs. 11 and 12, which conform to the simulation results. Figures 10(a) and 10(b) show the amplitude of the transmission and the polarization conversion ratio, respectively. In Fig. 11(a), the cross-polarization transmission peaks are at 9.76 GHz, 11.32 GHz, 13.02 GHz, and the co-polarization transmission peak is at 13.92 GHz. The polarization rotation angle and the ellipticity are shown in Figs. 12(a) and 12(b), respectively. These data are summarized in Table 2.

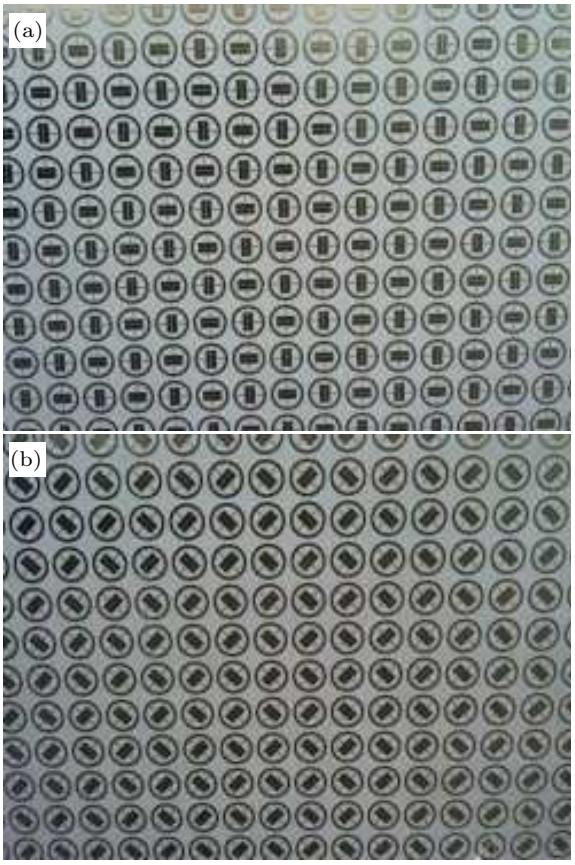


Fig. 9. (color online) Photographs of the fabricated sample ((a) top layer and (b) bottom layer).

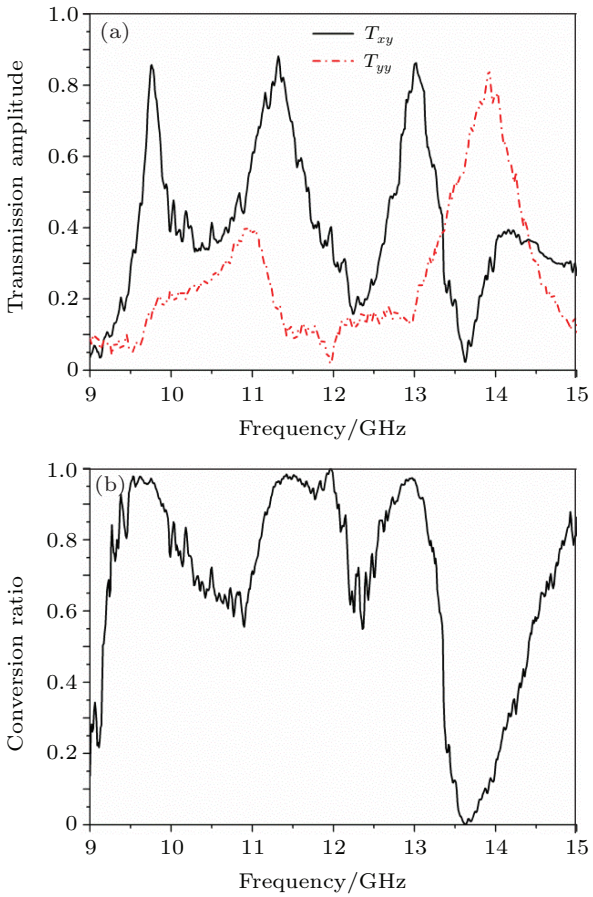


Fig. 10. (color online) (a) The measured transmission amplitude; (b) the measured polarization conversion ratio.

It is concluded from the data in Table 2 that the presented tri-band polarization angle-independent cross-polarization converter obtains a good performance with a low loss and high PCR. Therefore, the transmitted wave is almost purely linearly polarized and the polarization angel is rotated by nearly 90°. Furthermore, there is a co-polarization transmission at 13.92 GHz with a frequency selective effect, which gives the proposed design the potential to realize polarization-agile antennas. The difference between the simulation data in Table 1 and the measurement data in Table 2 are caused by machining and measurement errors.

Table 2. Summary of the measurement results of the chiral metasurface.

Frequency/GHz	9.76	11.32	13.02	13.92
$\|T_{xy}\|$	0.857	0.881	0.862	0.307
$\|T_{yy}\|$	0.15	0.17	0.188	0.844
PCR	0.97	0.964	0.955	0.117
$\psi/(^\circ)$	80.02	79.09	77.69	20
$\eta/(^\circ)$	−0.01	0.126	−3.07	−0.55

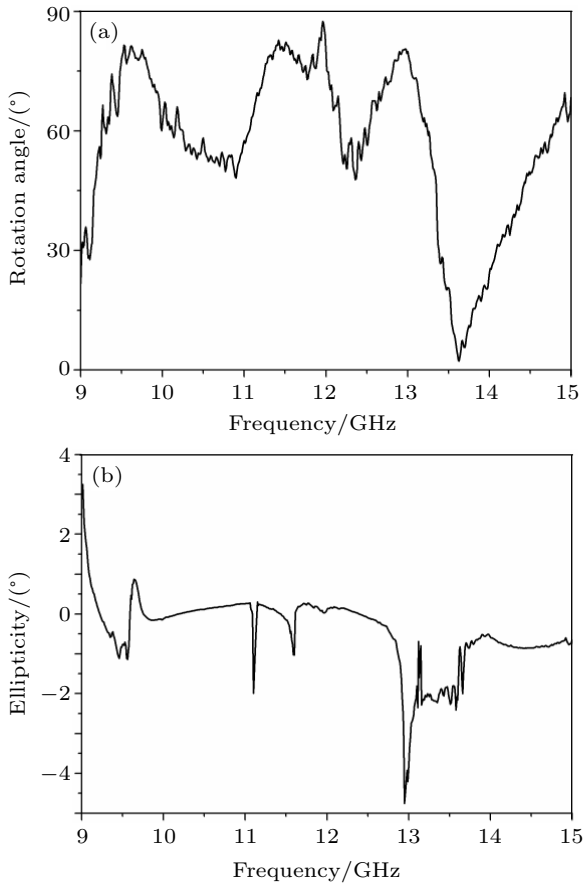


Fig. 11. (a) The polarization rotation angle; (b) the ellipticity.

4. Conclusion

In conclusion, we have proposed a bilayered chiral metasurface with $C4$ rotation symmetry to realize a tri-band polarization angle-independent cross-polarization convertor. This cross-polarization convertor exhibits strong cross-polarization

transmission with a high efficiency (about 95%), a high PCR (more than 99%), and low loss at three separated frequencies. Furthermore, the proposed design transmits the co-polarization wave at a different frequency, such as a frequency selective surface. The analyses of the current distributions indicates that the strong cross-polarization transmission is mainly due to the electric dipole coupling. With these properties, the proposed 90° polarization rotator can be employed in polarization-agile antenna applications or in telecommunication applications.

References

[1] Francesco M and Alu A 2014 *Chin. Phys. B* **23** 47809
[2] He Q, Sun S L, Xiao S Y, Li X, Song Z Y, Sun W J and Zhou L 2014 *Chin. Phys. B* **23** 47808
[3] Cui T J, Smith D R and Liu R 2010 *Metamaterials Theory, Design, and Applications* (New York: London: Springer)
[4] Landy N and Smith D R 2013 *Nat. Mater.* **12** 25
[5] Xu H X, Wang G M, Qi M Q, Lv Y Y and Gao X 2013 *Appl. Phys. Lett.* **102** 193502
[6] Fan Y N, Cheng Y Z, Nie Y, Wang X and Gong R Z 2013 *Chin. Phys. B* **22** 067801
[7] Wang G D, Liu M H, Hu X W, Kong L H, Cheng L L and Chen Z Q 2014 *Chin. Phys. B* **23** 017802
[8] Lu L, Qu S B, Su X, Shang Y B, Zhang J Q and Bai P 2013 *Acta Phys. Sin.* **62** 153301 (in Chinese)
[9] Lu L, Qu S B, Shi H Y, Zhang A X, Zhang J Q and Ma H 2013 *Acta Phys. Sin.* **62** 208103 (in Chinese)
[10] Mutlu M, Akosman A E, Serebryannikov A E and Ozbay E 2011 *Opt. Lett.* **36** 1653
[11] Zhao Y and Alu A 2011 *Photonic and Phononic Properties of Engineered Nanostructures* (San Francisco: SPIE)
[12] Wang J F, Qu S B, Ma H, Xu Z, Zhang A X, Zhou H, Chen H Y and Li Y F 2012 *Appl. Phys. Lett.* **101** 201104
[13] Yu N F and Capasso F 2014 *Nat. Mater.* **13** 139
[14] Sun S, He Q, Xiao S, Xu Q, Li X and Zhou L 2012 *Nat. Mater.* **11** 426
[15] Hao J, Yuan Y, Ran L, Jiang T, Kong J A, Chan C T and Zhou L 2007 *Phys. Rev. Lett.* **99** 063908
[16] Zhu L, Meng F Y, Dong L, Fu J H, Zhang F and Wu Q 2013 *Opt. Express* **21** 32099
[17] Shi H, Zheng S, Zhang A and Jiang Y 2013 *Frequenz* **68** 271
[18] Liu D Y, Luo X Y, Liu J J and Dong J F 2013 *Chin. Phys. B.* **22** 124202
[19] Zuo Y, Shen Z X and Feng Y J 2014 *Chin. Phys. B* **23** 34101
[20] Ye Y Q and He S 2010 *Appl. Phys. Lett.* **96** 203501
[21] Shi H, Zhang A, Zheng S, Li J and Jiang Y 2014 *Appl. Phys. Lett.* **104** 034102
[22] Li Z F, Mutlu M and Ozbay E 2013 *J. Opt.* **15** 023001
[23] Chuss D T, Wollack E J, Pisano G, Ackiss S, U-Yen K and Ng M W 2012 *Appl. Opt.* **51** 6824
[24] Mutlu M and Ozbay E 2012 *Appl. Phys. Lett.* **100** 051909
[25] Huang C, Ma X L, Pu M B, Yi G W, Wang Y Q and Luo X G 2013 *Opt. Commun.* **291** 345
[26] Pfeiffer C and Grbic A 2013 *Appl. Phys. Lett.* **102** 231116
[27] Cheng Y Z, Nie Y, Wang X and Gong R Z 2013 *Appl. Phys. A-Mater* **111** 209
[28] Cheng Y Z, Nie Y, Cheng Z Z, Wu L, Wang X and Gong R Z 2013 *J Electromagnet Wave* **27** 1850
[29] Shi J H, Liu X C, Yu S W, Lv T T, Zhu Z, Ma H F and Cui T J 2013 *Appl. Phys. Lett.* **102** 191905
[30] Wang B, Zhou J, Koschny T, Kafesaki M and Soukoulis C M 2009 *Journal of Optics A-Pure and Applied Optics* **11** 114003
[31] Menzel C, Rockstuhl C and Lederer F 2010 *Phys. Rev. A* **82** 053811